Available online at www.sciencedirect.com

ScienceDirect

journal homepage: www.elsevier.com/locate/he

Hydrogen production by glycerol steam-reforming over nickel and nickel-cobalt impregnated on alumina

*Esteban A. Sanchez, Raúl A. Comelli**

Instituto de Investigaciones en Catálisis y Petroquímica, INCAPE (FIQ-UNL, CONICET), Santiago del Estero 2654, S3000AOJ Santa Fe, Argentina

ARTICLE INFO

Article history:
Received 17 October 2013
Accepted 6 December 2013
Available online 4 January 2014

Keywords:
Hydrogen
Glycerol
Catalytic steam reforming
Cobalt–Nickel catalysts

ABSTRACT

Hydrogen is a clean energy carrier, and its utilization will reduce environmental problems related to fossil fuels one. Biomass is an inexhaustible renewable source to generate biocompounds. Glycerol, obtained from a crescent biodiesel industry, is an abundant biosubstrate to produce hydrogen. The steam reforming of glycerol was studied employing $4Ni/Al_2O_3$, $4Co–4Ni/Al_2O_3$, and $12Co–4Ni/Al_2O_3$ catalysts at 300, 500, and 700 °C, 1 atm, 10 h^{-1} WHSV, 6:1 water:glycerol molar ratio (WGMR), 0.17 ml min^{-1} glycerol solution feed flow rate and time-on-stream 8 h. The main product obtained was H_2, followed by CO_2, CO, and CH_4 in smaller proportion. Co promotes H_2 production and unfavors CO_2 generation when temperature decreases; CH_4 formation is observed at higher temperature. A low Co loading produces the largest H_2 and CO_2 amounts at the lowest temperature. A high Co loading improves H_2 production at lower temperature, but this does not occur at high temperature.

1. Introduction

There is a growing interest to employ the hydrogen as an energy carrier, mainly by the possibility of improve the current energy scene, and to reduce the environmental problems related to greenhouse gas emissions from utilization of non-renewable fossil fuels [1]. Furthermore, the continuous decrease of fossil fuel reserves and the increment of crude oil prices promoted the necessity to obtain renewable raw materials to generate clean energy by a sustainable way [2], contributing to improve the actual environmental condition [3]. Most of new technologies applied to energy production in European Union countries, USA, and the Asia-Pacific region, are directed to develop processes to transform raw materials derived from biomass into chemicals with high added value and also more economical and clean fuels [4].

In recent years, significant advances were obtained in order to use biocompounds, obtained from renewable biomass sources, in different industrial processes. Biodiesel, a mixture of methyl esters of fatty acids is produced by transesterification of vegetable oils using simple alcohols such as methanol or ethanol [5]; glycerol is obtained as the main byproduct. It was estimated that the glycerol amount obtained from biodiesel production will have a rapid increase in coming years in world, and it represents a problem because glycerol excess will not be easily absorbed by the future market with the increasing biodiesel demand [6]. There is a crescent

* *Corresponding author*. Tel.: +54 0342 4571164x2732; fax: +54 0342 4531068.
E-mail address: rcomelli@fiq.unl.edu.ar (R.A. Comelli).

0360-3199/$ – see front matter
http://dx.doi.org/10.1016/j.ijhydene.2013.12.067

interest for glycerol transformation because it comes from renewable resources, it is abundant, and it will allow a sustainable environmental development. Glycerol is a very convenient bio-renewable substrate to produce hydrogen, which can be used as a renewable and clean fuel in fuel cell, as a raw material to obtain chemicals and food products, in industrial processes such as ammonia production and Fischer-Tropsch synthesis [5], and to produce electricity [7].

Current processes for hydrogen production are based on catalytic reforming of hydrocarbons. In recent years, the possibility to obtain H_2 by reforming of glycerol has been widely investigated, because they are efficient processes to employ the excess of glycerol coming from the biodiesel industry [8]. Steam reforming of glycerol shows a great interest due to its operational characteristics and it is possible to obtain adequate reaction efficiency.

The glycerol steam reforming has been extensively investigated using supported catalysts with transition metals of VIII group, such as Pt, Pd, Ru, Rh, Co, and Ni, showing the last one an adequate activity during reaction. Using monometallic and bimetallic catalysts of Pt and Ni impregnated on Al_2O_3–SiO_2, Ni reached the best performance at 900 °C and WGMR 9:1, with 80% H_2 selectivity [9]. With Ni on MgO–Al_2O_3, an adequate calcination temperature favored the interaction with metallic phase, increasing catalytic activity [10]. Using Ni/Al_2O_3, the H_2 selectivity was strongly affected by reaction temperature, increasing at high temperature [11]; the best H_2 yield was 65% of the maximum theoretical value [12]. Ni/Al_2O_3 catalysts are susceptible to deactivation by carbon deposition, but their low costs made interesting investigate the possibility to improve the catalytic properties by addition of a promoter. Only a few studies employed Co/Al_2O_3 catalysts to produce H_2 by steam reforming [5,13,14], whereas Co–Ni/Al_2O_3 bimetallic catalysts were used in processes such as methane dry reforming [15], glycerol aqueous phase reforming [16], glycerol steam reforming [2], and acetol steam reforming [17].

In the present paper, the H_2 production by glycerol steam reforming was evaluated using Ni catalysts impregnated on Al_2O_3, adding Co as a promoter in order to analyze the catalytic performance under standardized operating conditions. Characterization of materials was performed by N_2 adsorption, X-ray diffraction (XRD), and Fourier-Transform infrared spectroscopy (FTIR).

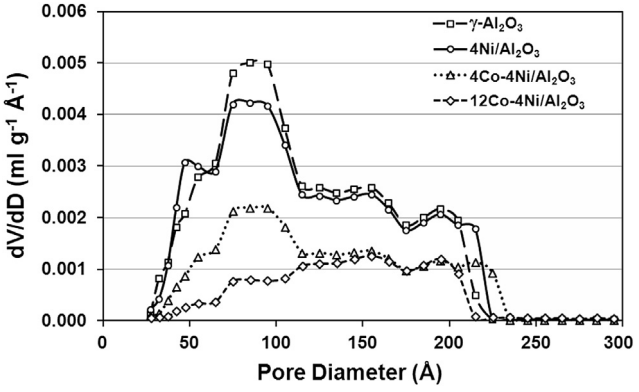

Fig. 1 – Pore-size distribution for Ni and Co–Ni catalysts, and γ-Al_2O_3 support. Samples calcined at 500 °C for 3 h in 50 ml min^{-1} air flow and reduced at 300 °C (Ni) and 400 °C (Co) for 3 h in 100 ml min^{-1} H_2 flow.

2. Experimental

2.1. Catalyst preparation

Catalysts containing either Ni or Co–Ni on alumina were prepared following the incipient wetness impregnation technique. The base material was a commercial sample of γ-Al_2O_3 (CK-300 Akzo Nobel, 199 m^2 g^{-1}, 0.51 cm^3 g^{-1}, and 35–80 mesh), which was calcined at 600 °C for 3 h in 50 ml min^{-1} air. Different solutions were prepared using nickel nitrate hexahydrate (Anedra) and sodium cobaltonitrite (Sigma) as precursors of Ni and Co species, respectively; concentrations were adequate to obtain 4 wt% Ni, and 4 and 12 wt% Co loadings. Impregnated samples were placed in a desiccator at room temperature for 4 h and then were dried in an oven at 110 °C for 12 h. Samples were identified as yCo-xNi/Al_2O_3, being "x" and "y" the Ni and Co loadings, respectively. Finally, catalysts were calcined at 500 °C for 3 h in 50 ml min^{-1} air.

2.2. Catalyst characterization

Prepared catalysts were characterized by N_2 adsorption, XRD, and FTIR being equipments and conditions previously reported [18]. Previous characterization, samples were reduced for 3 h in 100 ml min^{-1} H_2 at 300 and 400 °C for Ni and Co containing catalysts, respectively.

2.3. Catalytic measurements

Catalytic behavior of prepared materials was evaluated during the glycerol steam reforming using a system previously described [18]. A 50 wt% glycerol (Cicarelli) aqueous solution fed by a Cole Parmer 74900 syringe pump, and He as carrier gas were fed to the vaporizer. For catalytic test, 500 mg of reduced catalyst were placed into quartz reactor, being operating conditions 300, 500, and 700 °C, atmospheric pressure, 10 h^{-1} WHSV, 6:1 WGMR, 0.17 ml min^{-1} glycerol solution flow rate, and total time of 8 h.

Reaction was monitored by gas chromatography, being details of equipments, columns, temperature programs, and detectors previously reported [19]. Non-condensable products were on-line analyzed by gas chromatography using a 1.9 m

Table 1 – Textural properties for γ-Al_2O_3 support, and Ni and Co–Ni impregnated catalysts.

Materials	S_{BET} (m^2 $g^{-1}_{support}$)	PV (ml $g^{-1}_{support}$)	PD_M (Å)
γ-Al_2O_3	195.1	0.4771	97.8
4Ni/Al_2O_3	182.5	0.4776	104.7
4Co–4Ni/Al_2O_3	85.7	0.2527	118.0
12Co–4Ni/Al_2O_3	59.3	0.1592	107.4

Pretreatment conditions: samples calcined at 500 °C for 3 h in 50 ml min^{-1} air flow, and reduced at 300 °C (Ni) and 400 °C (Co) for 3 h in 100 ml min^{-1} H_2 flow.

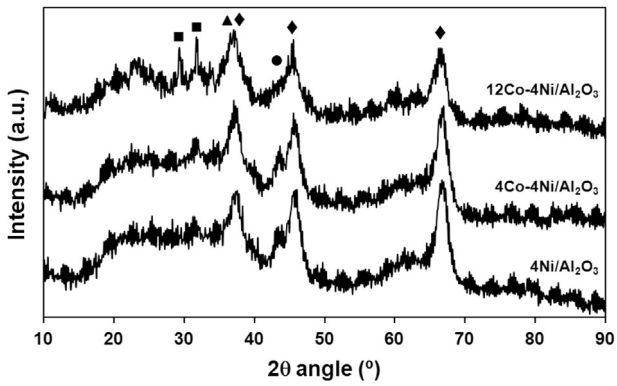

Fig. 2 – XRD patterns for Ni and Co–Ni catalysts. Samples calcined at 500 °C for 3 h in 50 ml min^{-1} air flow: (◆) $NiAl_2O_4$ and γ-Al_2O_3; (●) NiO; (■) Co_3O_4 and $NiCo_2O_4$; (▲) $CoAl_2O_4$.

long, 3.18 mm O.D. stainless steel packed column filled with Porapak Q 80/100 mesh (Alltech) in a Shimadzu GC-2014, and employing a thermal conductivity detector (TCD), being the operating program: 2 min at 40 °C, heating at 15 °C min^{-1} up to 100 °C, maintaining it 4 min. Calculations of composition in the gaseous non-condensable stream were previously described [18].

3. Results and discussion

3.1. *Catalyst characterization*

The pore size distributions for alumina support and reduced catalysts, showed in Fig. 1, were obtained from adsorption isotherms. By increasing the metal loading, the ratio dV/dD decreased, which is related to the increasing in deposited metal amount on γ-Al_2O_3. All materials displayed a marked mesopore presence, with no pores below 25 Å; it was clearly observed the macropores absence (pore diameters greater than 500 Å). The more mesopores quantities are between 60 and 120 Å, while remaining mesopores had sizes between 120 and 225 Å, except for catalyst with highest Co loading, which showed greater number of mesopores with sizes between 120 and 215 Å. Adsorption at low partial pressures corresponding to mesopores monolayer coverage, while the increase in adsorbed volume at relative pressures above 0.4 was related to mesopores filling [20]. The textural properties for calcined catalysts and alumina support, obtained from N_2 adsorption isotherms, are given in Table 1. The BET surface area (S_{BET}) and pore volume (PV) decrease for prepared catalysts by increasing the amount of impregnated precursor; it indicates correct metallic particles anchored to the pore structure on alumina support [5]. However, slightly differences were observed between 4Ni/Al_2O_3 and γ-Al_2O_3, whereas Co catalysts presented a more significant decrease by increasing metal loading. The decrease in material with the highest Co loading was possibly due to the high loading employed (12 wt %.), which generated larger metallic particles [20]. Analyzing the average pore diameter (PD_m), significant differences were not found between all catalysts, and they showed similar values to γ-Al_2O_3 without addition of metal precursors.

Fig. 2 shows XRD patterns for calcined catalysts. 4Ni/Al_2O_3 displayed the presence of γ-Al_2O_3 profile (data previously showed [18]), with a broad peak of medium intensity at 38°, together with well defined and higher intensity peaks at 46 and 68° [21]. Peak at 38° can also correspond to nickel aluminate spinel formation ($NiAl_2O_4$), which bands may appear at 46 and 68° in a lesser proportion [21]. It occurs because γ-Al_2O_3 has a pseudo-spinel structure with network structural characteristics similar to the formed by $NiAl_2O_4$ species [22]. The presence of a small peak at 43° appeared for 4Co–4Ni/Al_2O_3 and 4Ni/Al_2O_3, corresponding to NiO species and being weakly observed due to the low Ni loading [23]. Analyzing the Co catalysts patterns, two thin peaks appeared at 31 and 33° for 12Co–4Ni/Al_2O_3, being attributed to the presence of free cobalt oxide species (Co_3O_4), as well as Ni and Co spinel type structures ($NiCo_2O_4$) [5,16]. By increasing Co loading, peak at 37° decreased and became wider; it may be related to the presence of $CoAl_2O_4$ species overlapped with the already formed $NiAl_2O_4$ species [20].

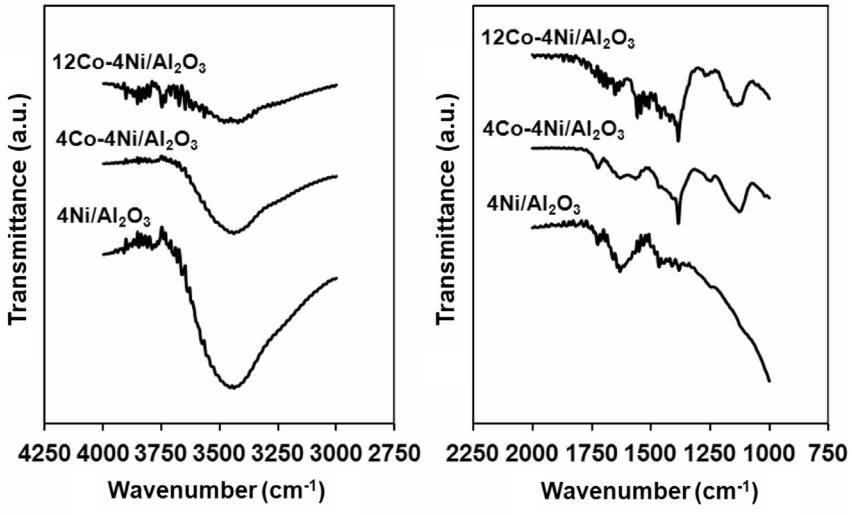

Fig. 3 – FTIR profiles for Ni and Co–Ni catalysts. Samples calcined at 500 °C for 3 h in 50 ml min^{-1} air flow.

The FTIR profiles for calcined catalysts are presented in Fig. 3. In the high frequency region (4000–3000 cm^{-1}), a strong and broad band at 3500 cm^{-1}, whose intensity decrease markedly with the increment in metal loading on the base material, was observed. A weak band at 3780 cm^{-1} was also showed, being weakly visible in catalyst with lower Co loading. The broad band at 3500 cm^{-1} correspond to interactions through hydrogen bonding between hydroxyls groups and chemisorbed water groups on γ-Al_2O_3 surface [24]. The 3780 cm^{-1} band was mainly attributed to acidic, neutral, and basic OH groups [25]. Throughout this region, Co and Ni metallic oxide species decrease the surface hydration degree on γ-Al_2O_3, causing an intensity decrease of the main band when the precursor loadings were increased [26,27]. In the low

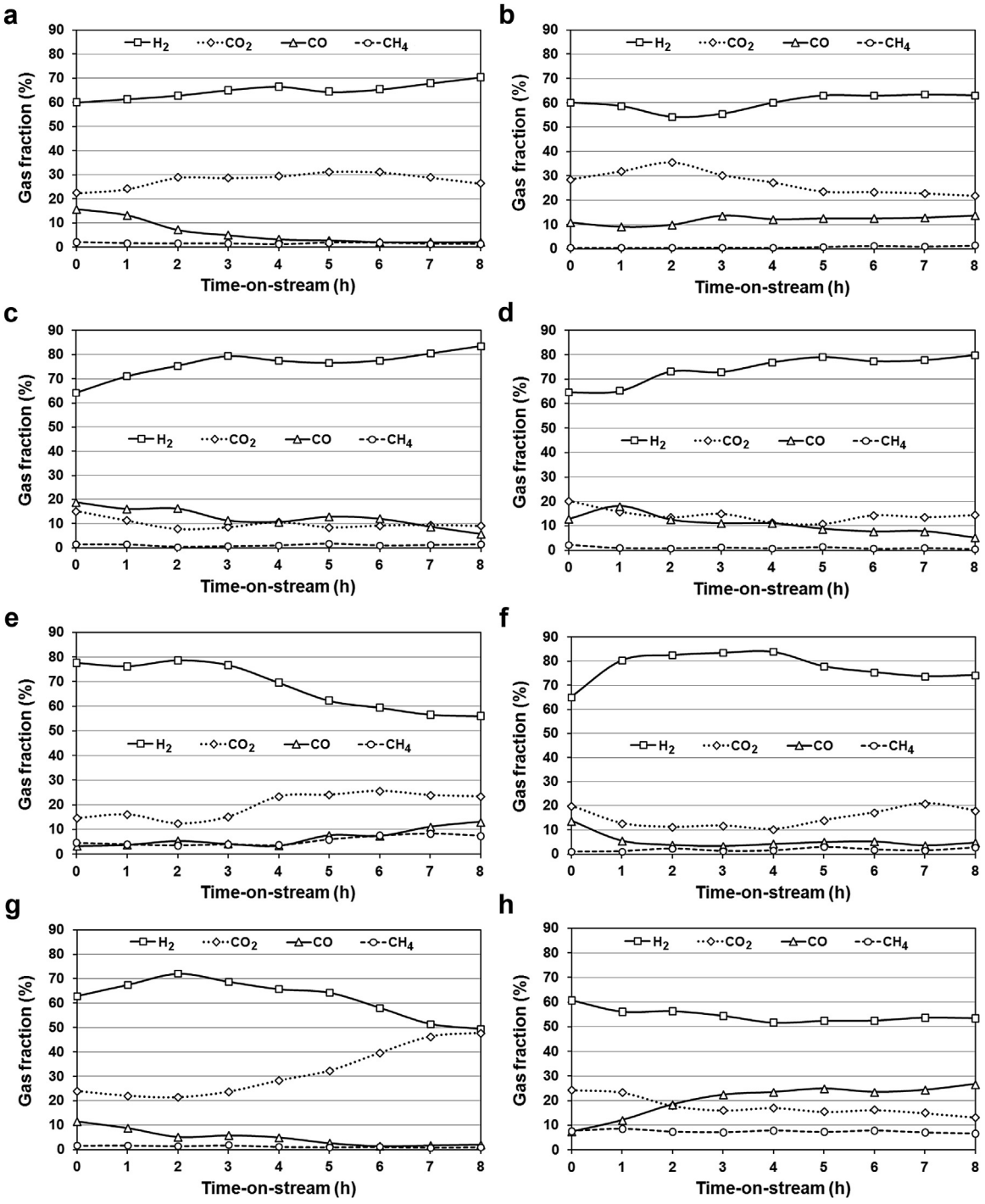

Fig. 4 – H_2, CO_2, CO, and CH_4 gas fractions obtained during the steam reforming of glycerol as a function of TOS. *Reaction conditions: atmospheric pressure, 10 h^{-1} WHSV, 6:1 water:glycerol molar ratio (WGMR), 0.17 ml min^{-1} glycerol solution feed flow rate, TOS 8 h.* a. 4Ni/Al_2O_3 at 500 °C. b. 4Ni/Al_2O_3 at 700 °C. c. 4Co–4Ni/Al_2O_3 at 300 °C. d. 4Co–4Ni/Al_2O_3 at 500 °C. e. 4Co–4Ni/Al_2O_3 at 700 °C. f. 12Co–4Ni/Al_2O_3 at 300 °C. g. 12Co–4Ni/Al_2O_3 at 500 °C. h. 12Co–4Ni/Al_2O_3 at 700 °C.

frequency region (2000–1000 cm^{-1}), a well defined band at 1630 cm^{-1} was observed for Ni catalyst, whose intensity decreases when Co loading increased to be less visible for 12Co–4Ni/Al_2O_3. A small band at 1440 cm^{-1} was also showed, being more important when the Co loading increased. A new and sharp band was displayed at 1100 cm^{-1} for 12Co–4Ni/Al_2O_3 and 4Co–4Ni/Al_2O_3, being not visible to 4Ni/Al_2O_3, and mainly attributed to Co_3O_4 and $NiCo_2O_4$ species. For 4Ni/Al_2O_3, species identification below 1700 cm^{-1} is difficult, although previous studies assigned 1620 and 1470 cm^{-1} bands to γ-Al_2O_3 support [28].

3.2. *Catalytic behavior*

Fig. 4 shows H_2, CO_2, CO, and CH_4 fractions eluted from glycerol steam reforming system for prepared catalysts at different operating temperatures. For 4Ni/Al_2O_3 at 500 °C (Fig. 4a), H_2 fraction presents an increase with TOS, from 60.0 to 70.4%, while the CO_2 one has slightly increase and then remains constant until 8 h. The CO fraction decreases from 15.6 to 2.0% in 5 h of reaction, whereas the CH_4 fraction presents low values during all TOS. With 4Ni/Al_2O_3 at 700 °C (Fig. 4b) the H_2 fraction decreases during the initial 2 h, from 60.2 to 54.3%, but then it shows a slight increase, exceeding the initial value. By contrast, the CO_2 fraction increases during the initial 2 h and then decreases at 21.7% at 8 h. This initial behavior can be associated to the time needed by the catalyst to reach the major activity, and then starting to decline by partial blockage of active sites by reactions that produce carbonaceous deposits ($H_2 + CO \rightarrow C + H_2O$) [15] and reactions that allow to generate CH_4 but consuming part of formed H_2 ($CO_2 + 4H_2 \rightarrow CH_4 + 2H_2O$) [29]. The CO and CH_4 fractions show a slight increase with TOS, reaching 13.7 and 1.4% at 8 h, respectively. The H_2:CO ratio indicates that in excess steam conditions, the Water Gas Shift (WGS) reaction is favored ($CO + H_2O \rightarrow H_2 + CO_2$) [2]. By increasing the reaction temperature, H_2 fraction improves more slowly than at lower temperature, and generating larger amounts of CO_2 and CO. Employing 4Co–4Ni/Al_2O_3 at 300 °C (Fig. 4c), the H_2 fraction increases from 64.3 to 83.6% with TOS; both CO_2 and CO fractions are similar and presents a slow decrease at 8 h (9.2 and 5.7%, respectively), being the CH_4 fraction low with TOS. For 4Co–4Ni/Al_2O_3 at 500 °C (Fig. 4d), behavior is similar to the same catalyst at 300 °C, indicating that the increment in temperature does not change the gaseous fractions. With 4Co–4Ni/Al_2O_3 at 700 °C (Fig. 4e), the H_2 fraction is higher at the beginning of reaction (77.5%) and stable for 3 h, but then decrease to 56.0% at 8 h; the CO_2 fraction increases from 14.5 to 25.6% during the first 6 h, but then remains constant up to 8 h. The CO and CH_4 fractions are constant and similar during the first 4 h (about 4.0%), and then increase slowly, reaching 13.1 and 7.5%, respectively. This catalyst has not marked differences between 300 and 500 °C, but at 700 °C the H_2 fraction becomes higher only during the first 2 h, and then decline rapidly. Furthermore, CO_2, CO, and CH_4 fractions increase with TOS, different to occurring at low temperatures. With 12Co–4Ni/Al_2O_3 at 300 °C (Fig. 4f), the H_2 fraction increases from 65.1 at 84.0% during 4 h, and then shows a slow decrease to 73% at 8 h; the CO_2 fraction decreases until 4 h and then presents a slightly recovery with TOS. The CO fraction decreases from 13.8 to 3.8% in 2 h, and then kept constant about 4.0–5.0%, while the CH_4 fraction is low in all TOS (2.0–3.0%). With 12Co–4Ni/Al_2O_3 at 500 °C (Fig. 4g), the H_2 fraction grows during the first 2 h from 62.9 to 72.1%, but then declines markedly to 49.4% at 8 h. The CO_2 fraction increases from 24.0 to 47.7% and the CO one decreases from 11.5 to 1.9% with TOS; similar at 300 °C, the CH_4 fraction remains low (1.0–1.8%). For 12Co–4Ni/Al_2O_3 at 700 °C (Fig. 4h), the H_2 fraction decreases from 60.7 to 57.7% at 4 h, and then remains constant; the CO_2 fraction decreases to 13.2% while the CH_4 one remains constant (6.5–8.5%). The CO fraction shows a significant increase, from 7.3 to 26.7 at 8 h; in this case the CO fraction exceeds the CO_2 one at 8 h. The increase in reaction temperature generates lower H_2 fractions, with major CO_2 fraction at 500 °C and CO one at 700 °C, observing the presence of a higher CH_4 fraction at 700 °C.

For prepared catalysts, the H_2 fraction is larger when reaction temperature is lower, whereas the CO_2 fraction is lower for each catalyst at the lowest temperature. The larger CH_4 fractions are reached during reactions at 700 °C (except for 4Ni/Al_2O_3), whereas the CO fractions tend to be higher reacting at 700 °C. In excess of steam, H_2, CO_2, and CO are the main gaseous products, with a lesser extent of CH_4 produced [5]. The large H_2 amount and the low CH_4 generation suggest that the CH_4 steam reforming is active at 700 °C ($CH_4 + H_2O \rightarrow 3H_2 + CO$) [30]. The Co addition promotes the H_2 production and unfavors the CO_2 generation by decreasing the reaction temperature; it can be explained considering reactions which consume that product ($CO_2 + 4H_2 \rightarrow CH_4 + 2H_2O$), while CH_4 formation is favored at higher temperature. The 4 wt% Co loading produces the largest H_2 and CO_2 fractions at low temperature, maintaining low levels of CO and CH_4. Increasing the Co loading from 4 to 12 wt%, the H_2 production increases slightly at low temperature, and displays more stability during the reaction. However, the H_2 production at 500 and 700 °C is lesser, showing a larger proportion of the remaining compounds.

4. Conclusions

Catalysts having 4 wt% Ni and 0, 4, and 12 wt% Co supported on γ-Al_2O_3 were prepared by incipient wetness impregnation. Materials displayed mesopores, without evidence of macropores. A correct anchor for metallic particles on γ-Al_2O_3, and the presence of larger ones on the Co containing catalysts, was showed. Typical γ-Al_2O_3 structures were identified while $NiAl_2O_4$ and NiO species were weakly detected, possibly by the low Ni loading employed. Free cobalt oxide species (Co_3O_4), Ni and Co spinel ($NiCo_2O_4$) and $CoAl_2O_4$ overlapped with $NiAl_2O_4$ were well evidenced. The γ-Al_2O_3 support has acidic, neutral, and basic hydroxyls, and Ni and Co metallic species decreased the surface hydration degree. Catalytic behavior of catalysts during the glycerol steam reforming produced H_2 as the main product, followed by CO_2, CO, and CH_4 in smaller proportions. Co promoted the H_2 production and unfavored the CO_2 generation by decreasing the reaction temperature, while the CH_4 formation was favored at higher temperature. The low Co loading produced the largest H_2 and CO_2 amounts at a low temperature, with low CO and CH_4. The high Co loading

improved the H_2 production at low temperature; it does not occur when reaction temperature was increased, showing an increment of the remaining generated compounds.

Acknowledgments

Authors thank to CONICET, CAI+D (UNL), and SECTeI (Secretaría de Estado de Ciencia, Tecnología e Innovación, Santa Fe) for financial support. Authors also thank to JICA (Japan International Cooperation Agency) by equipments for catalyst characterization donated to CENACA (Centro Nacional de Catálisis).

REFERENCES

[1] Navarro RM, Pena MA, Fierro JLG. Hydrogen production reactions from carbon feedstocks: fossil fuels and biomass. Chem Rev 2007;107:3952–91.
[2] Cheng CK, Foo SY, Adesina AA. Glycerol steam reforming over bimetallic Co-Ni/Al_2O_3. Ind Eng Chem Res 2010;49:10804–17.
[3] Ramirez de la Piscina P, Homs N. Biomass-derived alcohols as a renewable source for hydrogen production. In: Bismara Regitano d'Arce MA, Ferreira de Souza Vieira TM, Liborio Romanelli T, editors. Agroenergy and sustainability. Sao Paulo: EDUSP; 2009. pp. 241–55.
[4] Marshall AL, Alaimo PJ. Useful products from complex starting materials: common chemicals from biomass feedstocks. Chem Eur J 2010;16:4970–80.
[5] Cheng CK, Foo SY, Adesina AA. H_2-rich synthesis gas production over Co/Al_2O_3 catalyst via glycerol steam reforming. Catal Commun 2012;12:292–8.
[6] Pagliaro M, Rossi M. The future of glycerol. 2nd ed. Cambridge: RSC Publishing; 2010.
[7] Carter D, Ryan M, Wing J. The fuel cell industry review. Royston: Fuel Cell Today; 2012.
[8] Dieuzeide ML, Amadeo N. Thermodynamic analysis of glycerol steam reforming. Chem Eng Technol 2010;33:89–96.
[9] Adhikari S, Fernando SD, Haryanto A. Production of hydrogen by steam reforming of glycerin over alumina-supported metal catalysts. Catal Today 2007;129:355–64.
[10] Dieuzeide ML, Iannibelli V, Jobbagy M, Amadeo N. Steam reforming of glycerol over Ni/Mg/γ-Al_2O_3 catalysts. Effect of calcination temperatures. Int J Hydrogen Energy 2012;37:14926–30.
[11] Dou B, Rickett GL, Dupont V, Williams PT, Chen H, Ding Y, et al. Steam reforming of crude glycerol with in situ CO_2 sorption. Bioresour Technol 2010;101:2436–42.
[12] Douette AMD, Turn SQ, Wang W, Keffer VI. Experimental investigation of hydrogen production from glycerin reforming. Energy Fuels 2007;21:3499–504.
[13] Hu X, Lu G. Acetic acid steam reforming to hydrogen over Co-Ce/Al_2O_3 and Co-La/Al_2O_3 catalysts – the promotion effect of Ce and La addition. Catal Commun 2010;12:50–3.
[14] Hirai T, Ikenaga N, Miyake T, Suzuki T. Production of hydrogen by steam reforming of glycerin on ruthenium catalyst. Energy Fuels 2005;19:1761–2.
[15] Foo SY, Cheng CK, Nguyen TH, Kennedy EM, Dlugogorski BZ, Adesina AA. Carbon deposition and gasification kinetics of used lanthanide-promoted Co-Ni/Al_2O_3 catalysts from CH_4 dry reforming. Catal Commun 2012;26:183–8.
[16] Luo N, Ouyang K, Cao F, Xiao T. Hydrogen generation from liquid reforming of glycerin over Ni–Co bimetallic catalyst. Biomass Bioenergy 2010;34:489–95.
[17] Ramos MC, Navascués AI, García L, Bilbao R. Hydrogen production by catalytic steam reforming of acetol, a model compound of bio-oil. Ind Eng Chem Res 2007;46:2399–406.
[18] Sanchez EA, Comelli RA. Hydrogen by glycerol steam reforming on a nickel-alumina catalyst: deactivation processes and regeneration. Int J Hydrogen Energy 2012;37:14740–6.
[19] Sanchez EA, D'Angelo MA, Comelli RA. Hydrogen production from glycerol on Ni/Al_2O_3 catalyst. Int J Hydrogen Energy 2010;35:5902–7.
[20] Vaudry F, Khodabandeh S, Davis ME. Synthesis of pure alumina mesoporous materials. Chem Mater 1996;8:1451–64.
[21] Zhu X, Huo P, Zhang Y, Cheng D, Liu C. Structure and reactivity of plasma treated Ni/Al_2O_3 catalyst for CO_2 reforming of methane. App Catal B Environ 2008;81:132–40.
[22] Lo Jacono M, Schiavello M, Cimino A. Structural, magnetic, and optical properties of nickel oxide supported on η- and γ-aluminas. J Phys Chem A 1971;75:1044–50.
[23] Auroux A, Monaci R, Rombi E, Solinas V, Sorrento A, Santacesaria E. Acid sites investigation of simple and mixed oxides by TPD and microcalorimetric techniques. Thermochim Acta 2001;379:227–31.
[24] Stoilova D, Koleva V, Cheshkova K. Infrared spectroscopic study of NO and NH_3 adsorption on alumina-supported nickel oxide catalysts. Z Phys Chem 2002;216:737–47.
[25] Knözinger H, Ratnasamy P. Catalytic aluminas: surface models and characterization of surface sites. Catal Rev Sci Eng 1978;17:31–70.
[26] Kapteijn F, Van Langeveld AD, Moulijn JA, Andreini A, Vuurman MA, Turek AM. Alumina-supported manganese oxide catalysts-I. Characterization: effect of precursor and loading. J Catal 1994;150:94–104.
[27] Kapteijn F, Singoredjo L, Andreini A, Moulijn J, Van Driel M, Ramis G. Alumina-supported manganese oxide catalysts II: surface characterization and adsorption of ammonia and nitric oxide. J Catal 1994;150:105–16.
[28] Turek A, Wachs I, DeCanio E. Acidic properties of alumina-supported metal oxide catalysts: an infrared spectroscopy study. J Phys Chem A 1992;96:5000–7.
[29] Zhou CH, Beltramini JN, Fan YX, Lu GQM. Chemoselective catalytic conversion of glycerol as a biorenewable source to valuable commodity chemicals. Chem Soc Rev 2008;37:527–49.
[30] Dou B, Dupont V, Rickett G, Blakeman N, Williams P, Chen H. Hydrogen production by sorption-enhanced steam reforming of glycerol. Bioresour Technol 2009;100:3540–7.